Journal of Marine Research, 59, 769–794, 2001

Early diagenesis of calcium carbonate in Long Island Sound sediments: Benthic fluxes of Ca^{2+} and minor elements during seasonal periods of net dissolution

by Mark A. Green[1,2] and Robert C. Aller[1]

ABSTRACT

The present study confirms the quantitative significance of carbonate dissolution for associated major and minor element solute fluxes in shelf deposits of temperate regions. Multiple measurement techniques all demonstrate that net dissolution of $CaCO_3$ dominates during winter in Long Island Sound sediments and results in large fluxes of Ca^{2+}, Sr^{2+}, and F^- out of the seafloor. Ca^{2+} fluxes averaged from 4 independent methods range from ~5 to ~13 mmol m^{-2} d^{-1} with highest flux occurring when surface deposits are most undersaturated with respect to common biogenic carbonates. A significant proportion of dissolution, 40–100%, results from oxidation of reduced metabolites such as FeS, NH_4^+, and Mn^{2+}. Results suggest that 90% of the $CaCO_3$ precipitated each year is dissolved, equivalent to a loss of ~90–190 g $CaCO_3$ m^{-2} yr^{-1}. Given the general similarity between Long Island Sound and other muddy coastal estuaries along the eastern coast of North America and elsewhere (e.g. Chesapeake Bay, Delaware Bay, Narragansett Bay, Buzzards Bay, Casco Bay), these relative flux measurements are likely to be indicative of much larger temperate regions.

1. Introduction

Studies in the coastal deposits of Long Island Sound (LIS) have shown that these sediments are sites of a dynamic yearly cycle of biogenic calcium carbonate diagenesis (Aller, 1982; Reaves, 1986; Green *et al.,* 1993; Green and Aller, 1998). A regularly observed pattern of wintertime net undersaturation and $CaCO_3$ dissolution in surficial regions is followed by late spring-summer periods of net supersaturation and $CaCO_3$ deposition. Unlike the deep-sea, where aerobic CO_2 production is the primary metabolic acid and conditions are often assumed near steady state, $CaCO_3$ dissolution in LIS is controlled by the time-dependent interplay among seasonal physical, chemical, and biological processes (Green and Aller, 1998). Quantifying dissolution in nearshore temperate deposits is difficult because of the dynamic nature of sedimentary processes and the restriction of dissolution to narrow zones near the sediment-water interface. However, knowledge of dissolution rates and pathways in these types of environments is important to

1. Marine Sciences Research Center, State University of New York at Stony Brook, Stony Brook, New York, 11794-5000, U.S.A.

2. *Present address:* Saint Joseph's College, Department of Marine Science, 278 Whites Bridge Road, Standish, Maine, 04084-5263, U.S.A. ***email: mgreen@sjcme.edu***

more fully understand the cycling of C in the coastal ocean, and the mechanisms whereby biogenic carbonates are preserved in the sedimentary record.

In the present study, dissolution of $CaCO_3$ is quantified in LIS surficial sediments over an entire winter-time 'cycle' of pore-water calcite and aragonite undersaturation using multiple redundant measures of net Ca^{2+} flux across the sediment-water interface. Sediment incubations, flux-core incubations, pore-water concentration gradients, and a simple transport-reaction model are used to constrain the flux of Ca^{2+} from LIS sediments during winter when pore waters are undersaturated with respect to calcite and aragonite (Green and Aller, 1998). An additional estimate of dissolution is made using regular seasonal losses of benthic foraminifera from sediments. Stoichiometric relations of the diffusive fluxes of F^- vs. Ca^{2+}, Sr^{2+} vs. Ca^{2+}, and F^- vs. Sr^{2+} are used to infer the likely reacting mineral phases: lo-Mg calcite, hi-Mg calcite, and aragonite, which differ in F^-, Sr^{2+}, and Ca^{2+} elemental ratios. Results confirm that a substantial fraction of the sedimentary pool of $CaCO_3$ in LIS sediments is turned over and dissolves each winter. It follows that sediments in other similar temperate estuaries are sites with comparable seasonal carbonate cycles and, when taken together, represent a quantitatively significant yet little recognized region of the ocean where large amounts of biogenic $CaCO_3$ are precipitated, dissolved, and recycled each year.

2. Station location and sampling

Time series sampling was conducted at a single station in central Long Island Sound (LIS) as part of the PULSE study (41° 10.03N, 72° 57.43W) during winter-spring 1993. A map of the study location is given in Green and Aller (1998). A similar sampling protocol occurred during each of 11 cruises separated by approximately 14-day intervals. The general location of the study site has been extensively studied in the past (e.g. Station NWC: Aller and Cochran, 1976; Aller, 1977, 1982; Benninger *et al.,* 1979; Station P: Green *et al.,* 1992, 1993, 1998; Green and Aller, 1998; Gerino *et al.,* 1998). Water depth at this station averages ~15 meters. Sediments are muddy, consist of ~2% organic carbon and $CaCO_3$ by weight, and have an average surface sediment (0–1 cm) porosity (ϕ) of ~0.8. A Soutar-type box corer (0.1 m^2) was used to collect bottom sediment and overlying water during each cruise. Sampling dates, corresponding progressive year days, and surface and bottom water temperatures are given in Table 1.

3. Methods

A detailed description of the methods used for field collection of sediment subcores, and pore- and overlying-water analysis of Cl^-, Ca^{2+}, Sr^{2+}, F^-, NH_4^+, Mn^{2+}, pH, total alkalinity, CO_3^{2-}, and overlying- and pore-water saturation states with respect to calcite and aragonite, Ω (Ω = IMP/K'_{sp}; where IMP = ion molar product of Ca^{2+} and CO_3^{2-}; K'_{sp} = stoichiometric equilibrium constant for calcite or aragonite), are given in Green and Aller (1998). Standard methods were used for all analyses and include: Cl^-: Radiometer

Table 1. Cruise date, corresponding year day, and surface and bottom water temperatures (°C).

Cruise	Cruise date	Year day	Surface water (°C)	Bottom water (°C)
Pulse 1	12/15/92	−16	6.0	6.6
Pulse 2	1/21/93	21	3.1	3.1
Pulse 3	2/8/93	39	0.8	1.5
Pulse 4	3/1/93	60	0.2	0.4
Pulse 5	3/22/93	81	1.0	0.1
Pulse 6	4/12/93	102	3.8	3.6
Pulse 7	4/26/93	116	7.7	4.6
Pulse 8	5/10/93	130	13.1	8.7
Pulse 9	5/24/93	144	11.1	7.8
Pulse 10	6/7/93	158	12.3	11.1
Pulse 11	6/28/93	179	18.6	15.8

CMT Cl^- Titrator; Ca^{2+}: Flame Atomic Absorption; Sr^{2+}: Furnace Atomic Absorption; F^-: ion selective electrode and standard addition; NH_4^+: flow injection analysis; Mn^{2+}: formaldoxime; and pH: combination electrode calibrated with pH 4 and 7 NBS-traceable buffers.

Multiple techniques were used to measure Ca^{2+} flux across the sediment-water interface during each cruise. These methods include diffusive-transport model Ca^{2+} fluxes predicted from surficial pore-water profiles using Ficks First Law ($J\text{-}Ca^{2+}_{diff}$), directly measured Ca^{2+} fluxes into water overlying whole-core incubations ($J\text{-}Ca^{2+}_{dm}$), Ca^{2+} production fluxes inferred from sediment incubations ($J\text{-}Ca^{2+}_{inc}$), and model estimates based on simple transport-reaction model fits to measured pore-water Ca^{2+} profiles in their entirety ($J\text{-}Ca^{2+}_{mod}$). Use of redundant measures allows for evaluation of the assumptions inherent in each method and thus inference of processes controlling fluxes, places maximum constraints on the true magnitudes of fluxes, and helps identify the best overall measurement approaches.

a. Br-tracer estimates of solute transport

Several of the methods used to measure Ca^{2+} flux require an understanding of processes controlling solute transport rate (diffusive vs. biologically enhanced). For this study, time-series changes in spiked Br^- concentrations in water overlying intact sediment cores were used to quantify mass flux of Br^- (J_{Br}) into sediments and transport rate, D_{Br}, during each cruise (Martin and Banta, 1992). Previous work shows that Br^- is effectively conservative in surficial marine pore-water relative to overlying water concentrations and is an appropriate nonreactive tracer for estimating transport (Mackin *et al.,* 1988).

One butyrate subcore was collected along with overlying water during each sampling date (Table 1), fitted with o-ring sealed caps, and kept at *in situ* temperature for transport back to the lab. Cores were aerated and continuously stirred with small stirring motors. Overlying water was spiked with ~0.5 g KBr (yielding an initial Br^- concentration of 2–4 mM) and aliquots analyzed for Br^- in a time series for three days. The Br^-

concentrations as a function of time in overlying water of Br^- spiked cores were compared to theoretical estimates of Br^- loss from a finite volume of water overlying sediment, as predicted from a one-dimensional, diffusive transport model assuming no reaction (explicit finite difference scheme checked with exact analytical solution). Observed loss rates of Br^- were quantified using a constant transport coefficient and compared to that expected from molecular diffusion. The expected molecular diffusion coefficient (D_s^{Br}) for Br^- was calculated according to the equation:

$$D_s^{Br} = \phi^2 D_o^{Br} \tag{1}$$

Where, ϕ = porosity at $z = 0$ cm, and D_o^{Br} is the free solution diffusion coefficient for Br^- corrected for *in situ* temperature and viscosity using the Stokes Einstein relation (Li and Gregory, 1974). When the value of D_s^{Br} determined using Eq. (1) accurately modeled the *measured* change in Br^- concentration in spiked flux cores, simple molecular diffusion was assumed to be the dominant transport process for all solute species (i), and Eq. (1) was used to estimate D_s^i for Ca^{2+}, Sr^{2+}, and F^- using the solute-specific D_o from Li and Gregory (1974; e.g. D_o^{Ca}). Transport coefficients greater than those based on simple molecular diffusion were assumed to result from increases in transport at the sediment water interface by activities of benthic organisms. In this case, a quasi-diffusive or apparent-diffusive term (D_{app}) equal to the measured Br^- transport was used to describe transport of Ca^{2+}, Sr^{2+}, and F^-.

b. Diffusive flux based on pore-water gradients

Fick's first law of diffusion (Berner, 1980), was used to calculate fluxes of Ca^{2+}, Sr^{2+}, and F^- from sediment pore-water profiles during each cruise (e.g. J-Ca^{2+}_{diff}). Two-point gradients (dC/dz) from 0.0–0.5 cm during cruises 1–3, and from 0.0–0.25 cm during cruises 4–11 were used to calculate vertical diffusive flux according to:

$$J^i_{diff} = -\phi_0 D^i_s (dC/dz) \tag{2}$$

where, ϕ_0 = porosity at $z = 0$, D_s^i = whole sediment diffusion coefficient for solute species i (measured as described in section *a*), and dC/dz = solute concentration vertical gradient. Porosity was measured using the standard equation:

$$\phi = \omega * \rho_s / (\omega * \rho_s + (1 - \omega)\rho_\omega) \tag{3}$$

where ω = weight fraction H_2O, ρ_s = sediment density assumed to be 2.65 g solid cc-sediment^{-1}, and ρ_ω = water density assumed to be 1.02 g cm^{-3} H_2O^{-1}.

c. Directly measured flux-core incubations

Short-term changes in solute concentration as a function of time in water overlying sediment cores were used to directly measure mass flux of Ca^{2+} (J-Ca^{2+}_{dm}) across the sediment-water interface during each cruise (Mackin and Swider, 1989). One butyrate

core-liner (9.5 cm I.D.) was used to remove sediment along with overlying water from a box core during each cruise. The core was sealed with o-ring fitted caps on both top and bottom. Overlying water (~600–800 mL) was aerated with an aquarium pump through a small sampling port and continuously stirred with small, battery-operated stirring motors. Overlying water samples (30 ml) were removed in a time series for 3–4 days at ~12 hour intervals. The flux of Ca^{2+} from sediments was estimated by dividing the slope of the line of incubation time vs. $\Sigma \Delta M(t)$ by the area of the flux core (area = 71 cm^2), where:

$$\Sigma \Delta M(t) = [C(t) - C_c(t - \Delta t)]V_o \tag{4}$$

and, $C(t)$ = solute concentration at time t, $C_c(t - \Delta t)$ = corrected solute concentration in the previous sample and, V_o = volume of overlying water. Ca^{2+} was measured by EGTA titration as described by Tsunogai *et al.* (1968) with a precision of ~0.2%. EGTA was standardized each day against a Long Island Sound seawater standard (Cl^- = 422 mM) and sample concentrations of Ca^{2+} (C_s) calculated as:

$$C_s = Ca^{2+}_{std}/V_{EGTA;std} * V_{EGTA;sample} \tag{5}$$

Where, Ca^{2+}_{std} = the standard calcium concentration (7.95 mM), $V_{EGTA;std}$ = volume EGTA necessary to titrate standard, and $V_{EGTA;sample}$ = volume of EGTA necessary to titrate sample.

d. Sediment incubations and production flux estimates

Short-term sediment incubation experiments (24–72 hr) were used to measure net rates of Ca^{2+} production from 0–2 cm and from 2–4 cm and used to estimate the corresponding production fluxes (J-Ca^{2+}_{inc}). All incubations were performed by completely filling 25 mL plastic scintillation vials with largely undisturbed sediments from 0–2 and 2–4 cm and storing without air-contact in anoxic sediments. Incubated sediment vials were stored at *in situ* temperatures and sampled in a time series for 1–3 days with time zero values determined immediately at the onset of the incubations. Production rates of NH_4^+ and Mn^{2+} were also calculated using sediment incubations and used to estimate production flux (see Discussion). A more detailed explanation of the field collection of subcores, the incubation method, and the analytical techniques for solute analysis are described in detail in Green and Aller (1998).

Production of Ca^{2+}, NH_4^+, and Mn^{2+} in closed incubations was corrected for adsorption using a linear adsorption coefficient, K, by the relationship:

$$K = (1 - \phi)/\phi x \rho_s x K^* \tag{6}$$

where, ϕ = weighted mean porosity from 0–2 and 2–4 cm, ρ_s = dry sediment density (assumed 2.65 g cm^{-3}), and K^* = the adsorption constant (cm^3 pore water g^{-1} dry sediment). Net production rates for Ca^{2+}, NH_4^+, and Mn^{2+} were multiplied by the factor $1 + K$ (Berner, 1980). Values of K^* were taken from Li and Gregory (1974).

e. Model estimates of dissolution rate and Ca^{2+} flux

An additional estimate of combined calcite and aragonite dissolution rate ($R' = R_{\text{calcite}} + R_{\text{aragonite}}$) and Ca^{2+} flux can be made by modeling the interval of the pore-water Ca^{2+} profiles (J-Ca^{2+}_{mod}) over the region where the largest gradients in dissolved Ca^{2+} were observed (0–8 cm). Local steady state can be assumed because the spatial scale of interest is small (usually <5 cm) and the processes being measured are rapid relative to the 14–21 day sampling time-scale. Net sedimentation was negligible over the 6 month duration of the study so that profiles are defined as a balance between transport and supply and can be evaluated using a single-layer transport-reaction model (Berner, 1980). The equation used here to describe the pore-water Ca^{2+} distribution is:

$$\partial C/\partial t = 0 = D_s(\partial C^2/\partial z^2) + R'_o e^{-\alpha z} \tag{7a}$$

where, C = pore-water solute concentration; z = spatial coordinate, origin fixed at the sediment water interface and positive into sediment; D_s = bulk sediment diffusion coefficient for Ca^{2+} calculated as described previously; R'_o = combined calcite and aragonite dissolution rate at $z = 0$ and α = attenuation coefficient.

There are large surficial Ca^{2+} gradients that reach near-constant values by ~5 cm during periods of the year dominated by undersaturation (encompassing cruises 2–9). The form of the reaction function chosen is consistent with the likely dominance of dissolution processes in a surficial region of highest acid production (metabolic, mineral reoxidation) and with attenuation of dissolution with depth. It also has advantages of mathematical simplicity. The assumption of steady state means that knowledge of a specific kinetic form (e.g. reaction order, rate constants) is not necessary to evaluate net reaction rates. Thus, Eq. 7a was solved with the boundary conditions:

$$z = 0,\ C = C_T \tag{7b}$$

$$z = z_{\max},\ dC/dz \rightarrow 0 \tag{7c}$$

where, C_T = Ca^{2+} at $z = 0$ cm.

The attenuation coefficient, α, for each cruise was estimated by taking the ratio of the integral of the Ca^{2+} production rate measured from 0–2 cm and 2–4 cm and adjusting the value of α until,

$$R'_{(0-2)}/R'_{(2-4)} = (1 - e^{-2\alpha})/(e^{-2\alpha} - e^{-4\alpha}) \tag{8}$$

where $R'_{(0-2)}$ and $R'_{(2-4)}$ are the average Ca^{2+} production rates measured over 0–2 and 2–4 cm in sediment incubations in units of μmol Ca^{2+} cm^{-3} sediment d^{-1}. Values for R'_o (Eq. 7a) were varied to fit the measured Ca^{2+} profiles using the estimated value for α. Ca^{2+} flux at steady state was determined through integration of reaction rate over the modeled interval (0–8 cm).

f. Foraminifera abundance as an indicator of dissolution

Significant losses of total (live and dead) benthic foraminifera assemblages in LIS correlate with periods of pore water undersaturation during winter (Green *et al.,* 1993; 1998). Because of their small size, the pristine appearance of live individuals, and their extremely high densities in most coastal temperate deposits, calcareous foraminifera (lo-Mg calcite) are ideal "indicator" organisms in the study of shallow-water carbonate dissolution processes (Murray and Alve, 1999). Foraminifera abundance was quantified in surficial sediments during each of the 11 PULSE cruises and used as a biological tracer of $CaCO_3$ dissolution.

Three butyrate subcores (4.5 cm I.D.) were removed from the box core, extruded upward, and sectioned at intervals of 0–0.25 cm, 0.25–0.5 cm, 0.5–0.75 cm, 0.75–1.0 cm, 1.0–1.5 cm, 1.5–2.0 cm, 2.0–3.0 cm, and 3.0–5.0 cm. After gentle mixing by hand, ~3-cm^3 subsamples from each interval were placed into each of three pre-weighed plastic scintillation vials and fixed with 10 mL of 0.3% gluteraldehyde made up in 3.0% NaCl solution. In the laboratory, prior to identification, samples were stained with Rose Bengal following the procedure of Walton (1952), lightly vortexed to ensure even stain distribution, and sieved through a 62-μm mesh screen after 24 hours. All foraminifera (both living and dead) were enumerated under a disecting microscope. Aside from the absence of stain indicator, dead foraminifera were distinctly translucent relative to the nearly transparent appearance of live individuals and often showed visual evidence of dissolution.

4. Results

a. Thermodynamic predictions of saturation states

Detailed patterns of the calcite/aragonite saturation states in surface sediments in LIS during winter can be found in Green and Aller (1998). For the purposes of this paper, a plot of the depth interval-weighted mean $\Omega_{calcite}$ and $\Omega_{aragonite}$ from 0–5 cm as a function of sampling time is presented and clearly shows the strong time-dependent variability of calcite and aragonite saturation states in surficial LIS pore waters (Fig. 1). Average pore-water saturation states vary regularly from saturated or supersaturated conditions during cruise 1, to increasing degrees of undersaturation during cruises 2–6, before slowly migrating back toward saturation and supersaturation during cruises 7–11. Pore waters are more undersaturated with respect to aragonite during each cruise owing to its greater solubility (Morse, 1983). The period during which the spring phytoplankton bloom was deposited to sediments is also indicated in Figure 1. Deposition of the bloom and an increase in anaerobic ΣCO_2 production appears largely responsible for progression of pore-waters toward saturation and supersaturation during the spring and early summer (Green and Aller, 1998).

b. Pore-water solutes

Pore-water concentration profiles for Ca^{2+}, Sr^{2+}, and F^- during each PULSE cruise are given in Green and Aller (1998). Profiles of Ca^{2+} to be modeled here are presented in

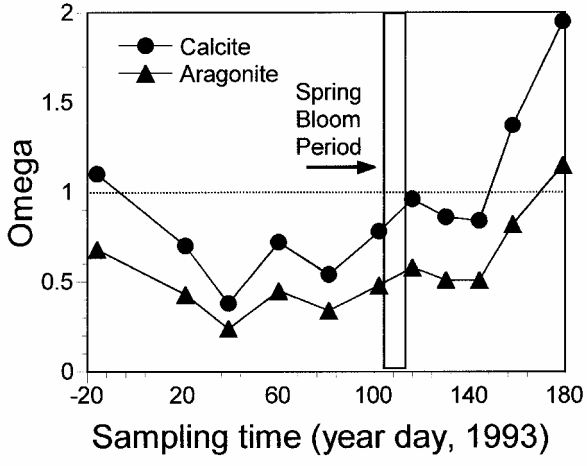

Figure 1. Comparative plot of the depth-integrated (0–5 cm) pore-water saturation state of calcite (closed circles) and aragonite (closed triangles) during PULSE cruises of winter-spring 1993.

Figure 2 (solid lines). Interstitial concentrations of Sr^{2+} and F^- follow relative patterns similar to those of Ca^{2+}. In general, there are relatively low excess pore water concentrations (normalized to Cl^-) for each of these solutes during late fall and early winter, followed by increasing excesses that reach maximum values during mid-winter cruises, before decreasing to low concentrations during warming temperatures and the onset of saturated and supersaturated conditions.

c. Pore water solute transport coefficients

Rates of solute transport in pore waters were estimated for each cruise from Br^- incubation flux cores and used to calculate transport coefficients for Ca^{2+}, Sr^{2+}, and F^-. Br^- transport during PULSE cruises 1–8 in Br^- spiked flux cores was controlled by simple molecular diffusion and modeled using molecular diffusive coefficients for Br^- (D_s^{Br}). Flux estimates of pore-water solutes during these cruises were derived using molecular diffusive transport coefficients based on Eq. (1), where in this case D_o was the free solution diffusion coefficient for either Ca^{2+}, Sr^{2+}, or F^- corrected for *in situ* temperature and viscosity (Li and Gregory, 1974).

During cruises 9–11 transport of Br^- was 3–6 times that based on simple molecular diffusion, indicative of an enhanced transport process. Br^- spiked cores were sectioned following the last incubation time point (~3 days) and showed near-linear interstitial water Br^- gradients during each of the 11 cruises. However, the depth of Br^- penetration into sediments during cruises 9–11 ranged from 4–8 cm compared with penetration depths of 2–3 cm during cruises 1–8. The near-linear gradient, deeper sediment penetration, and the rapid transport coefficient necessary to model changes in overlying water Br^- suggest an *enhanced* transport process during cruises 9–11 when particle bioturbation activity and

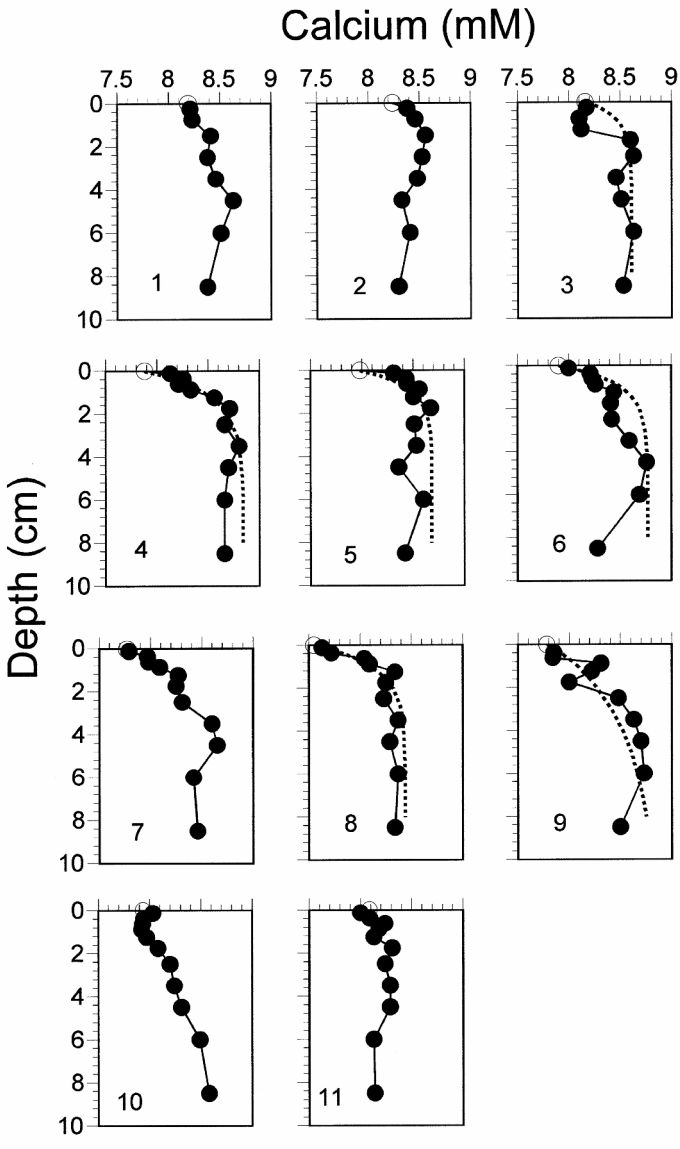

Figure 2. Pore-water distributions of Ca^{2+} during PULSE cruises 1–11. The open circle is the bottom water Ca^{2+} concentration. Model fits to pore-water data are shown by dotted lines.

benthic populations clearly increased (Gerino *et al.,* 1998). Thus, an apparent-diffusive term (D_{app}) equal to the flux core Br^- transport rate was used to describe transport of Ca^{2+}, Sr^{2+}, and F^- during cruises 9, 10 and 11. Transport based on nonlocal exchange (η) processes may also have resulted in nondiffusive subsurface injection. Use of a D_{app} coefficient is reasonable when multiple biogenic transport processes mimic random eddy

Table 2. Surface sediment diffusion coefficients for Ca^{2+}, Sr^{2+}, and F^- estimated from Br^- flux estimates and Eq. 1. The bold coefficients during cruises 9–11 are apparent diffusion transport rates (D_{app}) which result from an enhanced transport due to the competing transport processes of benthic organisms. Diffusive flux estimates based on surficial pore water profiles are also given (J_{diff}) for Ca^{2+}, Sr^{2+}, and F^-. Units are mmol m^{-2} d^{-1} for Ca^{2+} and μmol m^{-2} d^{-1} for Sr^{2+} and F^-. Negative fluxes are out of the sediment. The symbol * denotes that no data are available.

Cruise	$D_s Ca^{2+}$	$D_s Sr^{2+}$	$D_s F^-$	$J_{diff} Ca^{2+}$	$J_{diff} Sr^{2+}$	$J_{diff} F^-$
Pulse 1	0.25	0.25	0.46	−0.16	*	−29.8
Pulse 2	0.22	0.22	0.40	−0.99	−8.1	−80.7
Pulse 3	.021	0.21	0.38	−0.07	−31.1	−49.7
Pulse 4	.021	0.21	0.38	−3.46	−72.0	−127
Pulse 5	0.21	0.21	0.39	−4.82	−27.8	−214
Pulse 6	0.24	0.24	0.44	−5.51	−125	−215
Pulse 7	0.25	0.25	0.45	−1.12	−181	−279.3
Pulse 8	0.27	0.27	0.49	−1.45	−67.4	−77.1
Pulse 9	**1.45**	**1.45**	**1.45**	−1.15	−73.3	−91.6
Pulse 10	**1.80**	**1.80**	**1.80**	−0.35	−39.3	−122
Pulse 11	**2.20**	**2.20**	**2.20**	−1.45	−99.6	−56

diffusion (Vanderborght *et al.,* 1977; Goldhaber *et al.,* 1977; Aller, 1978). This analogy is valid when biological reworking is limited to the near surface of the deposit, the scale length of transport is relatively small, the reactions of interest occur over the same scale, and only short time periods are considered. Transport coefficients for Ca^{2+}, Sr^{2+}, and F^- are given for each cruise in Table 2.

d. Diffusive flux based on pore-water gradients

Diffusive flux estimates (J_{diff}) based on Fick's first law of diffusion (Eq. 2) for Ca^{2+}, Sr^{2+}, and F^- were calculated from surficial pore water gradients of these solutes and are given in Table 2. There are similar time variations of the calculated fluxes of Ca^{2+}, Sr^{2+}, and F^- using this method: fluxes out of sediment increase to maximum values between cruises 5 and 7 (−5.5 mmol Ca^{2+} m^{-2} d^{-1}, ~ −181 μmol Sr^{2+} m^{-2} d^{-1}, −279 μmol F^- m^{-2} d^{-1}), before decreasing during later cruises (Fig. 3a, b). In each case, fluxes increase by a factor of 2–3 in winter-spring cruises, during and following the 4–8 week period in which pore-waters were undersaturated (Fig. 1).

e. Flux-core incubation estimates

Short-term changes in solute concentration as a function of time in water overlying aerated sediment cores were used to directly measure Ca^{2+} flux ($J\text{-}Ca^{2+}_{dm}$) across the sediment water interface during each cruise. EGTA titration resolved ~30–50 μmol changes in overlying water Ca^{2+} over relatively short time-scales. Ca^{2+} fluxes determined by this method are given in Table 3 and are plotted relative to other methods in Figure 3a. Flux core estimates increase to maximum release values of ~ −20 mmol Ca^{2+} m^{-2} d^{-1} during middle cruises. During cruises 9–11 in late spring, however, fluxes reversed

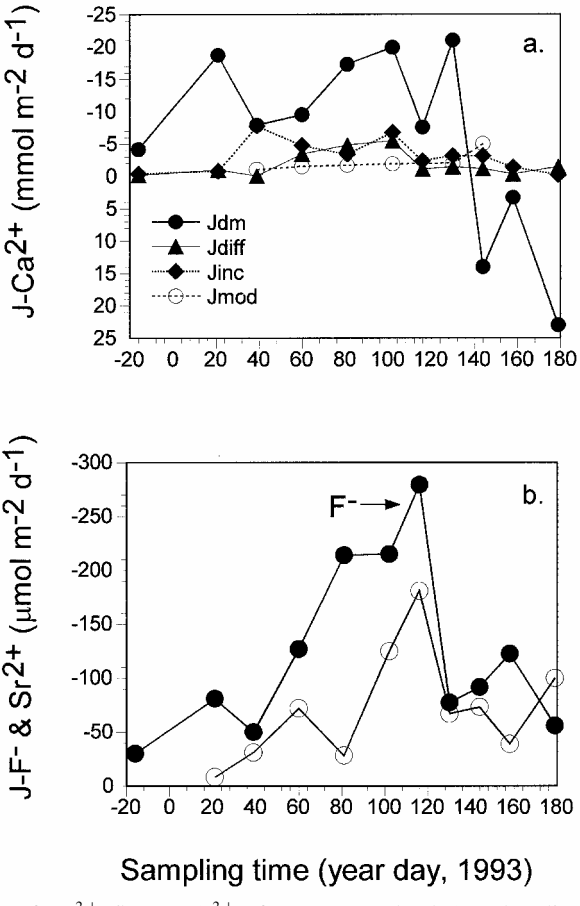

Figure 3. Estimates of Ca^{2+} flux (J-Ca^{2+}) from Long Island Sound sediments using multiple measurement techniques. Negative fluxes represent release from sediments and positive fluxes are into sediments.

dramatically and yielded an average net flux of 13.4 ± 9.9 mmol Ca^{2+} m^{-2} d^{-1} *into* sediments. The increases in Ca^{2+} in aerated water overlying flux cores during PULSE 4, 5, and 6 are shown in Figure 4 and are representative of linear increases in flux core Ca^{2+} documented during periods dominated by undersaturation.

f. Sediment incubations and production flux estimates

Ca^{2+} production rates from 0–2 cm and 2–4 cm sediment incubations were used to calculate Ca^{2+} production flux (J-Ca^{2+}_{inc}). Net rates were corrected for adsorption using a linear adsorption coefficient, K. Average porosity (0–2 and 2–4 cm), values for K, corrected Ca^{2+} production rates, and Ca^{2+} production fluxes are presented in Table 3. A value of 1.4 was used for K^*-Ca^{2+} (Li and Gregory, 1974). There was no detectable

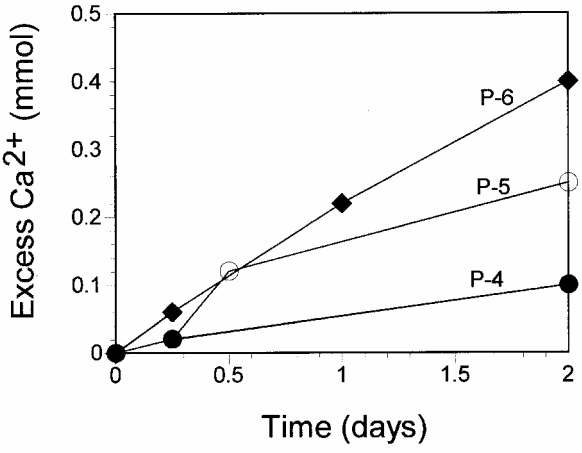

Figure 4. Plots of excess Ca^{2+} in water overlying aerated flux cores during PULSE cruises 4, 5, and 6.

production of Ca^{2+} from the 2–4 cm interval in cores collected during PULSE cruises 1, 2, 10, and 11. The combined production flux (0–4 cm) ranges from a high during PULSE 3 of ~ -8.0 mmol Ca^{2+} m^{-2} d^{-1} to an average low of ~ -0.3 mmol Ca^{2+} m^{-2} d^{-1} during cruises 1 and 11. Estimates of Ca^{2+} flux based on closed incubations are shown relative to other methods in Figure 3a. Production of Ca^{2+} was generally only seen within the first ~24 hrs of incubation, after which a net loss of Ca^{2+} from incubated sediments was frequently observed. The high pH and anaerobic ΣCO_2 production within this surface zone resulted in enclosed sediments that became rapidly supersaturated with respect to carbonate minerals, typically resulting in no *net* dissolution within ~48 hours after the start of incubations (Green and Aller, 1998).

Table 3. Directly measured Ca^{2+} flux estimates from flux core incubations (J_{dm}) and production flux estimates from sediment incubations (J_{inc}; 0–2, 2–4, & 0–4 cm). Ca^{2+} production rates (adsorption corrected; $K^* = 1.4$) in units of μmol cc sed^{-1} d^{-1} are also shown for the 0–2 and 2–4 cm intervals. All flux units are mmol m^{-2} d^{-1}. Negative fluxes are out of the sediment and positive fluxes are in.

Cruise	$J_{dm}Ca^{2+}$	Porosity 0–2 cm	Porosity 2–4 cm	K-Ca^{2+} 0–2 cm	K-Ca^{2+} 2–4 cm	Ca^{2+} Prod. (0–2 cm)	Ca^{2+} Prod. (2–4 cm)	$J_{inc}Ca^{2+}$ (0–2 cm)	$J_{inc}Ca^{2+}$ (2–4 cm)	$J_{inc}Ca^{2+}$ (0–4 cm)
Pulse 1	−4.18	.79	.73	0.99	1.37	0.02	N.D.	−0.4	0	−0.4
Pulse 2	−18.7	.78	.74	1.1	1.30	0.04	N.D.	−0.8	0	−0.8
Pulse 3	−7.9	.80	.74	0.93	1.30	0.35	0.04	−7.0	−0.8	−7.8
Pulse 4	−9.5	.82	.75	0.81	1.24	0.20	0.04	−4.0	−0.8	−4.8
Pulse 5	−17.3	.82	.75	0.81	1.24	0.15	0.02	−3.0	−0.4	−3.4
Pulse 6	−19.9	.83	.75	0.76	1.24	0.30	0.04	−6.0	−0.8	−6.8
Pulse 7	−7.6	.82	.76	0.81	1.17	0.05	0.07	−1.0	−1.4	−2.4
Pulse 8	−21	.81	.75	0.87	1.24	0.15	0.02	−3.0	−0.2	−3.2
Pulse 9	14	.74	.75	1.30	1.24	0.12	0.04	−2.4	−0.8	−3.2
Pulse 10	3.32	.82	.73	0.81	1.37	0.07	N.D.	−1.4	0	−1.4
Pulse 11	23	.81	.76	0.87	1.17	0.01	N.D.	−0.2	0	−0.2

Table 4. Model parameters of attenuation coefficient (α), R_o (μmol cc sed^{-1} d^{-1}), and model estimates of Ca^{2+} flux in units of mmol m^{-2} d^{-1}.

Cruise	Alpha (α)	R_o	$J_{mod}Ca^{2+}$
Pulse 1	—	—	—
Pulse 2	—	—	—
Pulse 3	1.1	0.13	−1.0
Pulse 4	0.85	0.15	−1.5
Pulse 5	1.0	0.20	−1.7
Pulse 6	1.1	0.25	−1.9
Pulse 7	—	—	—
Pulse 8	1.0	0.24	−2.0
Pulse 9	0.5	0.3	−5.0
Pulse 10	—	—	—
Pulse 11	—	—	—

g. Model predictions of Ca^{2+} flux

Pore water Ca^{2+} profiles and model fits of pore-water data based on Eq. 7a–c are given in Figure 2 (dashed line). There are no model generated Ca^{2+} profiles for cruises 1, 2, 10, and 11 owing to our inability to generate a value for α as there was no measurable Ca^{2+} production in the 2–4 cm interval of incubations during these cruises (Table 3). In addition, the measured Ca^{2+} production in the 0–2 cm interval during cruise 7 was extremely low relative to other cruises and similar to production in the 2–4 cm interval (0.05 μmol Ca^{2+} cc sed^{-1} d^{-1}) and did not allow a model fit. In general, there is good agreement between model and measured Ca^{2+} profiles during cruises 3–9, suggesting that methods used to calculate R'_o, α, and transport are reasonable. The most obvious discrepancy between actual and predicted Ca^{2+} is seen in the surficial 1 cm of sediment during cruise 3, where model estimates are greater than measured concentrations. Undetected transport factors or local limitations on reactive $CaCO_3$ could explain the lack of accumulation of pore water Ca^{2+} relative to model estimates. Ca^{2+} fluxes from the modeled 0–8 cm ($J\text{-}Ca^{2+}_{mod}$) interval were calculated by integration of the best fit reaction function (α derived from incubation experiments) assuming a porosity of 0.85. Values of α, R'_o, and Ca^{2+} flux are given in Table 4. Model estimated Ca^{2+} fluxes range from a low of −1.0 mmol Ca^{2+} m^{-2} d^{-1} during PULSE 3 to a high of −5.0 mmol Ca^{2+} m^{-2} d^{-1} during PULSE 9 and are shown in Figure 3.

h. Foraminifera inventories

As seen in Figure 5, total foraminifera inventories (0–5 cm) decrease significantly following the onset of calcite undersaturation (Fig. 1). Mean inventories decrease from a cruise 2 high of 857 foraminifera cm^{-2} ($\pm$166) through a cruise 6 minimum of 292 foraminifera cm^{-2} ($\pm$39). The period of deposition of the spring phytoplankton bloom to underlying sediments is noted and correlates with a rapid increase in the total foraminifera inventory (predominantly live individuals). Other studies by Buzas (1965) and Green *et al.*

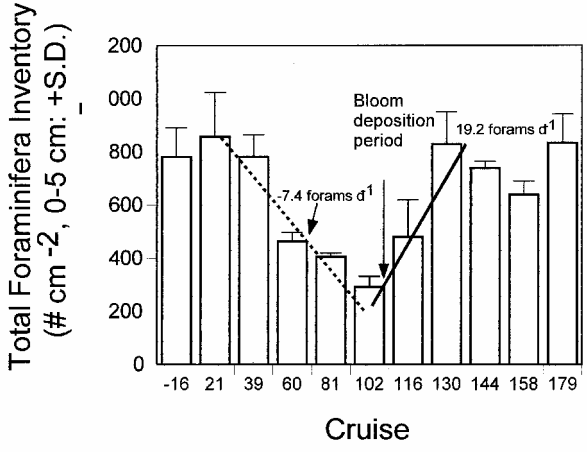

Figure 5. Total foraminifera inventories in surface sediments (0–5 cm) during each PULSE cruise. Dashed and solid lines represent least-squares regression during periods of rapid foram loss (dashed line) and rapid foram increase (solid line).

(1993) also show the strong dependence of foraminifera spring recruitment on bloom deposition in LIS sediments.

5. Discussion

It is widely emphasized that significant $CaCO_3$ dissolution is a largely deep-sea phenomenon related to both overlying water saturation state and sedimentary metabolic activity. Despite this, it has been repeatedly observed that quantitatively significant amounts of biogenic $CaCO_3$ produced in marine environments shoreward of the shelf break dissolves in both terrigenous and carbonate sediments underlying waters saturated or supersaturated with respect to carbonate minerals (Alexandersson, 1978; Milliman, 1974; Aller, 1982; McNichol *et al.,* 1988; Morse *et al.,* 1985; Reaves, 1986; Walter and Burton, 1990; Rude and Aller, 1991). Documentation of the diagenetic cycling of $CaCO_3$ in these shelf regions is important and aids in the current understanding of the cycling of C and the preservation of $CaCO_3$ in the sedimentary record. The present study confirms the quantitative significance of carbonate dissolution for associated major and minor element solute fluxes in shelf deposits, and further constrains the magnitudes and seasonal dynamics of net reaction patterns.

a. Ca^{2+} flux from Long Island Sound sediments

All methods of flux measurement used here indicate that a regular seasonal pattern of net release of Ca^{2+} occurs during periods of sedimentary undersaturation with respect to carbonate minerals (Fig. 3; Tables 2–4). In general, the relative magnitude of different estimates of Ca^{2+} flux during the period dominated by undersaturation (cruises 1–9) are:

directly measured flux-core ($J\text{-}Ca^{2+}_{dm}$) > incubation predicted ($J\text{-}Ca^{2+}_{inc}$) > diffusion predicted ($J\text{-}Ca^{2+}_{diff}$) > model predicted ($J\text{-}Ca^{2+}_{mod}$), with mean flux values over the period of 15, 3.6, 2.1, and 2.2 mmol $m^{-2}\,d^{-1}$, respectively. The larger average model predicted flux (2.2 mmol $m^{-2}\,d^{-1}$) relative to diffusion predicted (2.1 mmol $m^{-2}\,d^{-1}$) is driven largely by the high model estimated flux during cruise 9 (5.0 mmol $m^{-2}\,d^{-1}$). During most cruises diffusion predicted flux is greater than model estimates. Despite the inter-method differences, the mean Ca^{2+} flux calculated using all four techniques show that dissolution of $CaCO_3$ is an active process in Long Island Sound sediments during late fall, winter, and early spring, with Ca^{2+} flux increasing substantially when pore waters become undersaturated with respect to calcite and aragonite (Figs. 1, 3).

Differences between various flux estimates result from differences in assumptions associated with each method and method-specific error. For example, diffusive flux estimates depend on both accurate resolution of surficial Ca^{2+} concentration gradients and quantification of the transport regime. These estimates are probably most accurate during mid-winter when the largest pore-water Ca^{2+} gradients exist and transport is physically controlled (Fig. 2). However, based on the discrepancy between the measured flux and the gradient-predicted estimates, it appears that surface core sectioning at 0.25 cm during the middle cruises still underestimated the Ca^{2+} gradients (dC/dz) just below the S.W.I., thus yielding diffusive estimates less than directly measured fluxes. Sediment incubation experiments likely provide minimum estimates of Ca^{2+} flux because metabolite buildup during sediment enclosure causes calcite/aragonite undersaturation to be relieved rapidly in the absence of transport. If dissolution kinetics are high-order (Keir, 1980; Walter and Morse, 1985; Jahnke *et al.,* 1994), then small changes in Ω during incubations would result in large underestimation of dissolution flux. Uncertainty in modeling both the transport regime (e.g. nonlocal irrigation) and depth-dependent reaction functions impact Ca^{2+} flux estimates derived from overall pore water profiles. Directly measured flux estimates ($J\text{-}Ca^{2+}_{dm}$) are ~6× those based on other methods but probably provide the best overall estimate of Ca^{2+} flux. Artifacts could exist if subcores used for the flux incubations were not representative of typical Long Island Sound sediments during the sampling period, and if boundary layer transport was not well reproduced during stirring of overlying water. In this latter case, fluxes would likely be underestimates.

The sudden reversal in the direction of the directly measured Ca^{2+} flux in late spring (Fig. 3) correlates closely with the recruitment of shell-bearing benthos, such as foraminifera, following the spring phytoplankton bloom (Fig. 6; see: Buzas, 1965; Gerino *et al.,* 1998; Green *et al.,* 1993; Green, 1996). Using a test weight of 10 ± 4.8 μg $CaCO_3$ $foram^{-1}$ (Green *et al.,* 1993), an average addition of ~19 foraminifera $cm^{-2}\,d^{-1}$ to sediments (see Fig. 5) could result in Ca^{2+} uptake of ~19 mmol $Ca^{2+}\,m^{-2}\,d^{-1}$. The directly measured fluxes during cruises 9–11 indicate a maximum Ca^{2+} uptake of ~23 mmol $Ca^{2+}\,m^{-2}\,d^{-1}$ with an average of ~13 mmol $Ca^{2+}\,m^{-2}\,d^{-1}$, suggesting that

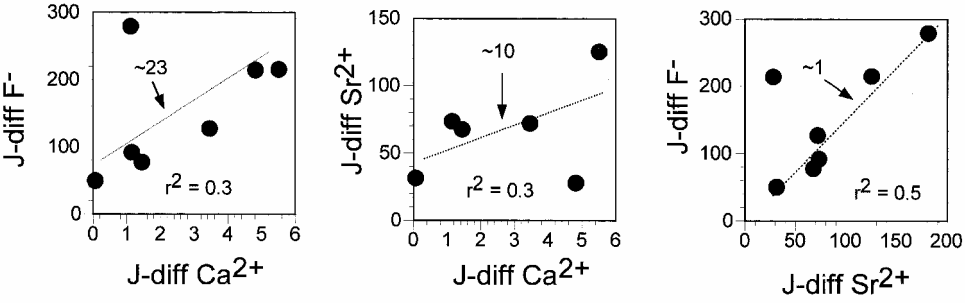

Figure 6. Ratios of diffusive flux (J_{diff}) estimates for F^-/Ca^{2+}, Sr^{2+}/Ca^{2+}, and F^-/Sr^{2+} during middle PULSE cruises when surface sediments were most undersaturated with respect to calcite and aragonite. Dashed lines represent least-squares fit to the data.

most or all of the net Ca^{2+} flux into sediments during this period could be accounted for by growth of benthic forams alone. The fact that the pore water concentration gradients do not demonstrate such a reversal in net flux at the same time probably indicates the direct extraction by shell-bearing benthos of Ca^{2+} from overlying water rather than from pore water, or, of course, systematic errors in measurements. Taken at face value, however, the various flux estimates imply a period of simultaneous dissolution (bulk sediment chemistry) and biogenic precipitation (local shell deposition) during the spring bloom and benthic recruitment, with an overall dominance of the latter process.

The inter-method differences documented in this study exemplify the importance of utilizing multiple measurement techniques when constraining benthic geochemical processes such as $CaCO_3$ cycling.

b. $CaCO_3$ mass loss

The average Ca^{2+} dissolution flux determined from all 4 solute-based methods during the period of the year characterized by undersaturation of pore water with respect to either aragonite or calcite (cruise 1–10, ~174 days) is equivalent to 5.1 ± 5.8 mmol Ca^{2+} m^{-2} d^{-1} (excluding the cruise 9–10 positive fluxes from J_{dm}), or 13 ± 7 mmol Ca^{2+} m^{-2} d^{-1}, if only the directly measured release fluxes are considered (cruise 1–8, 146 days). These estimates translate to annual average dissolution fluxes of 2.4 to 5.2 mmol m^{-2} d^{-1} respectively, and lie well within the range of observed oxygen fluxes (potential acid production) to the bottom at this site (~14 mmol m^{-2} d^{-1}). These Ca^{2+} fluxes are equivalent to a mass of 89 to 190 g $CaCO_3$ m^{-2} dissolved each year (FW $CaCO_3$ = 100 g/mol). If we assume that these quantities apply to the entire muddy region of LIS (~1792 km^2 or ~56% of total area; Bokuniewicz and Gordon, 1980), then at least ~1.6 to 3.4×10^{11} g $CaCO_3$ dissolves annually in LIS.

Based on Sanders' (1956) benthic community production rates, Aller (1982) calculated a minimum average annual $CaCO_3$ production due to macrofauna alone of ~1.8 mmol Ca^{2+} m^{-2} d^{-1} (67 g $CaCO_3$ m^{-2} yr^{-1}) in central LIS. Benninger *et al.* (1979) estimate a mean

sedimentation rate of ~290 g m^{-2} yr^{-1} near the present sampling site, suggesting that carbonate contents of ~20–25% should be observed if no dissolution were taking place and only macrofauna produced carbonate debris (Aller, 1982). In fact, only about 2–5% $CaCO_3$ actually accumulates. Our present dissolution flux estimates are therefore consistent with the loss on average of the vast majority of the shell debris formed (~90%), and indicate that given the magnitude of sediment accumulation, total benthic community shell production (mollusks, foraminifera) must be at least ~95 to 195 g $CaCO_3$ m^{-2} yr^{-1} in order to preserve ~2% carbonate. Given the similarity between LIS and numerous muddy estuary deposits along the eastern coast of N. America and elsewhere (e.g. Chesapeake Bay, Delaware Estuary, Narragansett Bay, Buzzards Bay, Casco Bay), these relative flux magnitudes and reaction balances are likely to be indicative of much larger temperate regions.

Ca^{2+} dissolution fluxes measured in this study are comparable with values reported from shallow water carbonate sediments and are generally 10–100 times greater than those estimated for the deep-sea. Rude and Aller (1991) used multiple techniques to estimate Ca^{2+} fluxes that ranged from −5 to −6 mmol m^{-2} d^{-1} in the shallow water carbonate muds of Florida Bay. In the Rodriquez and Tavernier bank sediments of the Florida Keys, Walters and Burton (1990) estimated Ca^{2+} fluxes of −1.0 to −19.0 mmol Ca^{2+} m^{-2} d^{-1} from mass loss of carbonate substrates incubated *in situ.* They report that roughly half of the annual carbonate production is dissolved each year. In the deep sea, Berelson *et al.* (1990) and Jahnke *et al.* (1994) used benthic flux chambers in regions of the Pacific to measure Ca^{2+} flux of −0.4 and −0.01 to −0.2 mmol Ca^{2+} m^{-2} d^{-1}, respectively. Hales (1995) described Ca^{2+} flux on the Ontong-Java Plateau of ~ −0.1 mmol Ca^{2+}, accounting for ~20–40% of the calcite supply to the seafloor in this region. More recently, Jahnke *et al.* (1997) used benthic flux chambers at stations ranging in depth from 790 to 3745 meters in California continental margin sediments to measure Ca^{2+} flux ranging from −0.9 to −2.9 mmol Ca^{2+} m^{-2} d^{-1}. Martin *et al.* (2000) measured Ca^{2+} flux by fitting a simple functional form to pore water data and determined fluxes of −0.16 and −0.14 to −0.47 mmol Ca^{2+} m^{-2} d^{-1} at sites B (3279 m) and G (4675 m) on the Ceara Rise.

c. Ca^{2+} flux based on loss of foraminifera

An additional constraint on net dissolution comes from measured seasonal changes in total foraminifera abundances in surface sediments (similar to method in Green *et al.,* 1993). Least squares regression through the period of decreasing foram (live + dead) inventories yields a significant slope of −7.4 foraminifera cm^{-2} d^{-1} (Fig. 5; $r^2 = 0.94$; $p = 0.007$). This loss of forams during the 81 day period translates to an average net Ca^{2+} flux of 7.4 mmol Ca^{2+} m^{-2} d^{-1}, assuming as done previously, that an average empty test weight for natural mixed populations of LIS foraminifera is ~10 ± 4.8 μg $CaCO_3$ (Green *et al.,* 1993). Several studies have shown that production of foraminifera during winter is minimal relative to other periods of the year, with recruitment-production largely dependent on warming water and deposition of the spring phytoplankton bloom to sediments

(e.g. Buzas, 1965). Therefore, the net dissolution derived from total abundances (live + dead) as done here, probably corresponds closely to total (gross) foram dissolution during this time. Prorating the net loss over an annual cycle results in a minimum dissolution loss of ~1.6 mmol m^{-2} d^{-1} due to dissolution of forams alone. Green *et al.* (1993) reported a minimum average annual dissolution flux of Ca^{2+} due to forams alone of ~6 mmol Ca^{2+} m^{-2} d^{-1} based on modeling population changes during the period 1988–89 and is in general agreement with the value reported here. Presumably the cycle of foraminifera loss (dissolution) and foraminifera gain (production) shown in Figure 5 represents one period of a yearly steady-state system so that annually averaged, these two terms should be equal. If this is true, then if the period of recruitment documented in this study represents the major reproductive period for benthic forams in LIS then other periods of dissolution loss must occur sometime during the year to balance these two terms.

d. Dissolving mineral phases

Pore-water distributions of Ca^{2+}, Sr^{2+}, and F^- have been used to infer the dissolution or precipitation of specific carbonate mineral phases during diagenesis (Carpenter, 1969; Baker *et al.,* 1982; Morse and Mackenzie, 1990; Rude and Aller, 1991; Green *et al.,* 1992, 1998). In principle, stoichiometric relations of F^- vs. Ca^{2+}, Sr^{2+} vs. Ca^{2+}, and F^- vs. Sr^{2+} reflect the relative contribution of reacting minerals, each of which vary in their Sr^{2+}/Ca^{2+} and F^-/Ca^{2+} compositions. At steady state, the solute flux ratios of Sr^{2+}, Ca^{2+}, and F^- should also be determined by the net contribution of different reacting carbonate minerals (e.g., Rude and Aller, 1991). In the present study, ratios of the diffusive fluxes of Ca^{2+}, Sr^{2+}, and F^- from cruises 2–9 were used to indicate the likely dominant mineral phases dissolving when pore-waters were undersaturated with respect to both calcite and aragonite.

Ratios of diffusive flux estimates for Ca^{2+}, F^-, and Sr^{2+} yield values of ~23 (mmol/mol), ~10 (mmol/mol), and ~1 (mol/mol) for F^-/Ca^{2+}, Sr^{2+}/Ca^{2+}, and F^-/Sr^{2+}, respectively (Fig. 6, least squares fit). The Sr^{2+}/Ca^{2+} and F^-/Sr^{2+} flux ratios are comparable to what would be expected from a mostly aragonite source. For example, aragonite from Florida Bay (USA) have Sr^{2+}/Ca^{2+} and F^-/Sr^{2+} ratios ranging from 9–12 (mmol/mol) and 0.3–3.0 (mol/mol), respectively (Rude and Aller, 1991). A predominant aragonite source is also consistent with pore water concentration relationships over 0–7 cm, which indicate net Sr^{2+}/Ca^{2+} and F^-/Sr^{2+} reaction ratios of ~9 (mmol/mol) and ~1 (mol/mol) (Green and Aller, 1998). In addition, laboratory dissolution experiments using bulk surficial LIS muds indicate an average dissolving carbonate source with a Sr^{2+}/Ca^{2+} ratio of ~10 (Green *et al.,* 1998).

Aragonitic mollusc shells from both living and dead individuals are known to dissolve in LIS surface sediments. For example, dissolution pits have been observed on aragonitic shells of the protobranch deposit-feeder *Nucula annulata* and the mactrid suspension feeder *Mulinia lateralis,* common species in LIS sediments (Green, 1996; Aller, 1982). Glover and Kidwell (1993) showed that *Nucula* sp. readily dissolve when exposed to

undersaturated seawater. Presumably, the elevated Sr^{2+}/Ca^{2+} and F^-/Sr^{2+} ratios reported here reflect in part the dissolution of such aragonite source material.

In contrast, the F^-/Ca^{2+} ratio of 23.0 (mmol/mol) reported here is 2–4 times estimates of ratios in aragonite and high magnesian calcite, and ~40 times that expected for low magnesian calcite (Rude and Aller, 1991). This difference suggests that carbonate dissolution is unlikely to be the exclusive source of F^- and sole determinant of elemental ratios. In addition to its occurrence in carbonates, F^- is also abundant in Fe-oxides and can be released into solution during Fe reduction in surface sediments (Ruttenberg, 1990; Rude and Aller, 1993). The potential range of F^-/Sr^{2+} present in aragonites (0.3–3 mol/mol) is sufficiently large that the observed flux ratios of F^-/Sr^{2+}, F^-/Ca^{2+}, and Sr^{2+}/Ca^{2+} could reflect both a predominant aragonite carbonate source and a contribution to F^- flux from additional reactions such as Fe-oxide reduction. For example, up to 70% of the F^- flux reported here could be derived from Fe reduction while still maintaining a F^-/Sr^{2+} carbonate source ratio equivalent to 0.3 mol/mol. A F^-/Sr^{2+} source ratio of 0.3 mol/mol would represent the lower limit of the observed range for aragonite (0.3–3 mol/mol) documented in the literature (e.g. Rude and Aller, 1991). In addition, based on arguments made earlier, there must be a significant contribution of low Mg calcite foraminifera to dissolution fluxes. Therefore, although a substantial aragonite dissolution source seems likely (e.g., as required by Sr^{2+}/Ca^{2+}), other carbonates and reactions can be accommodated within the uncertainty of the stoichiometric constraints. Simultaneous precipitation can also remove solutes with a distribution coefficient different from that of a dissolving mineral. As a result, the net release of any given solute may depart from that produced from a simple congruent dissolution.

e. Kinetics of dissolution

Carbonate dissolution rates, R, depend on the departure of the solution from saturation such that: $R = k(1 - \Omega)^n$. Depending on mineralogy, the order of reaction, n, has been variously proposed as ~3–4.5 (Keir, 1980; Walter and Morse, 1985), or more recently, ~1 for bulk sedimentary carbonate in the deep sea (Hales and Emerson, 1997). The reaction constant, k, reflects solid phase properties such as grain size (Keir, 1980). Under conditions of local steady state and assuming that carbonate dissolution dominates Ca^{2+} reaction, then the relation of net Ca^{2+} flux to solution saturation state in underlying sediment should directly reflect the overall kinetics of dissolution:

$$J_{dm} = \int_0^{z^*} -\Phi k(1 - \Omega(z))^n dz \tag{9}$$

Aragonite debris apparently dominates the carbonate dissolution source in LIS deposits (Aller, 1982). Therefore, we examined the relation of the directly measured net Ca^{2+} flux (J_{dm}-Ca^{2+}) to the aragonite saturation state from 0–5 cm in underlying sediments during the period of net Ca^{2+} release from sediments (Pulse 1–8). Any depth-dependence of

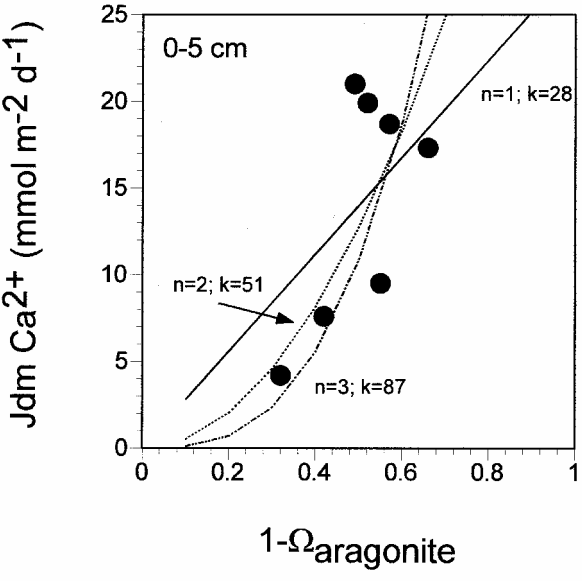

Figure 7. The relation of directly measured net Ca^{2+} flux (J_{dm}-Ca^{2+}) to the weighted-average aragonite saturation state (0–5 cm) during PULSE cruises 2–7. Reaction order, n, from 1–3 and rate constants, k, are shown and generally encompass the data according to the rate law, $R = k(1 - \Omega)^n$.

saturation states $(1 - \Omega(z))$ or reactivity, k, can greatly influence the total Ca^{2+} flux leaving the deposit (Eq. 9). In the present cases, however, there are relatively small depth variations in the $(1 - \Omega(z))$ function over the upper 5 cm (Green and Aller, 1998), and we found by comparing numerical integrations of measured $(1 - \Omega(z))$ that use of a simple average saturation state was an adequate approximation to the integral in Eq. (9). Possible depth variation in reactivity, k, could not be evaluated.

Although the scatter dictates no clear resolution regarding the exact reaction order, the relationship between directly measured fluxes and pore-water saturation states suggest that, in general, overall reaction orders of $n \sim 1$–3 encompass the present data (Fig. 7). Reaction order and rate constants for the fits shown from 0–5 cm lie between $n = 1$ ($k = 28$ mmol m^{-2} d^{-1}) and $n = 3$ ($k = 87$), with a value of $n = \sim 2$ ($k = 51$) best encompassing the data. Similar results were calculated from $(1 - \Omega(z))$ averaged from the upper 0–0.5 cm only, where dissolution is enhanced by strong acid production. Values of n in that case ranged between 1 ($k = 29$) and 3 ($k = 65$), with $n = \sim 2$ again best encompassing the data set ($k = 45$; data not shown). Subgrouping of flux and saturation data on the basis of temperature did not yield significant differences because of the small data set and restricted temperature range. The very general conclusions here are that bulk sediment values of k are relatively low (~0.5–1.6% d^{-1} $CaCO_3$ pool, assuming ~2% by weight total sediment) and that n may be lower than the frequently cited value of ~4.5.

f. Controls on saturation states

Neutralization of CO_2 produced from the aerobic degradation of carbon compounds accounts for up to 80% of the calcite dissolution and 100% of the aragonite dissolution in the deep sea (Emerson and Bender, 1981; Archer *et al.,* 1989; Berelson *et al.,* 1994; Hales *et al.,* 1994). In organic-rich, coastal marine deposits, anaerobic processes often dominate carbon remineralization and strong acids derived from secondary oxidation of anaerobic metabolites such as sulfide can be important reactants for carbonate dissolution. Seasonal changes in temperature and metabolic reactions are also important in temperate estuaries. During summer, warm water temperatures, relatively large amounts of labile carbon, increased microbial metabolism, and low concentrations of water column O_2, result in a dominance of anaerobic metabolism in sediments and migration of the oxic/anoxic boundary close to or above the sediment-water interface. O_2 penetration depths into sediments in central LIS during summer months, for example, are generally <1 mm (Mackin and Swider, 1989; Aller, 1994). High anaerobic production rates of CO_2 and alkalinity during this period results in pore waters which are saturated with respect to biogenic carbonates and reduced metabolites such as Fe-sulfides build-up in sediments (e.g. Goldhaber *et al.,* 1977; Aller, 1982; Green and Aller, 1998).

Conditions shift during winter so that cold water temperatures, relatively low concentrations of labile carbon, and decreased microbial metabolism typically result in a deepening penetration of O_2 into sediments, reaching 6–8 mm in central LIS deposits (Green, 1996). Greater penetration of O_2 results in an increased zone of oxidation for both carbon and reduced metabolites such as FeS, Mn^{2+}, and NH_4^+. Solid and dissolved reduced metabolite oxidation is related to $CaCO_3$ dissolution by reactions such as:

$$FeS + 9/4O_2 + 2CaCO_3 + 5/2H_2O \rightarrow 2Ca^{2+} + 2HCO_3^- + SO_4^{2-} + Fe(OH)_3 \quad (10)$$

$$NH_4^+ + 2O_2 + 2CaCO_3 \rightarrow NO_{3^-} + H_2O + 2HCO_3^- + 2Ca^{2+} \quad (11)$$

$$2Mn^{2+} + O_2 + 4CaCO_3 + 2H_2O \rightarrow 2MnO_2 + 4Ca^{2+} + 4HCO_3^- \quad (12)$$

The contribution of metabolite oxidation reactions to $CaCO_3$ dissolution in LIS can be inferred from time-dependent changes in solid phase pools (FeS) or differences between production reactions and observed fluxes across the sediment-water interface (Mn^{2+}, NH^{4+}). Net loss of FeS from surface sediments during cruises 1–5 corresponds to $\sim$0.05 μmol FeS cm^{-2} d^{-1} (Green and Aller, 1998). Provided that FeS loss was due to complete oxidation (not FeS_2 production), then according to Eq. 10, FeS oxidation could support a Ca^{2+} flux of ~ -1.0 mmol Ca^{2+} m^{-2} d^{-1}. This flux represents $\sim$20% of the Ca^{2+} released during this period based on the average flux determined from all four methods (5.1 mmol Ca^{2+} m^{-2} d^{-1}) or $\sim$8% of the directly measured Ca^{2+} flux. Oxidation of FeS_2, not accounted for here, would produce $\sim 3\times$ the H^+ per mole than oxidation of FeS alone.

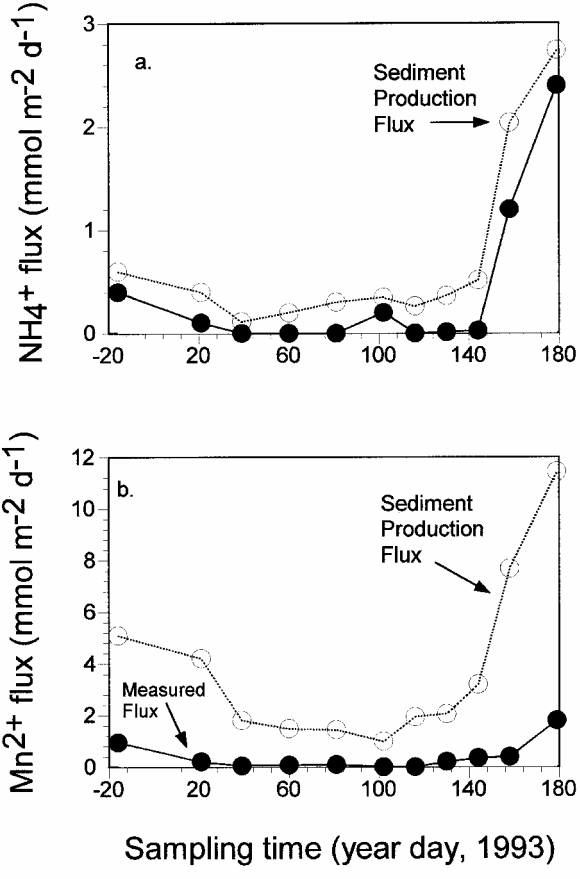

Figure 8. Comparative plots of production flux (J_{inc}) from sediment incubations with measured flux based on release to water overlying flux cores for (a) NH_4^+ and (b) Mn^{2+} during PULSE cruises.

In the case of reduced dissolved metabolites, the mean production flux (corrected for adsorption) for NH_4^+ and Mn^{2+} during cruises 2–9 (undersaturated conditions) is ~0.3 ± 0.1 and ~2.1 ± 1.0 mmol m^{-2} d^{-1} for NH_4^+ and Mn^{2+}, respectively (Fig. 8). During this period, there was no measurable release of either NH_4^+ or Mn^{2+} to water overlying retrieved cores. Assuming that all of the NH_4^+ and Mn^{2+} produced is oxidized in the sediment, then according to Eqs. 11 and 12, a Ca^{2+} flux of ~0.4–0.8 and ~2.2–6.2 mmol Ca^{2+} m^{-2} d^{-1} could result from NH_4^+ and Mn^{2+} oxidation, respectively. The combined contribution of ~2.6–7.0 mmol Ca^{2+} m^{-2} d^{-1}, corresponds to ~50–100% of the method-averaged Ca^{2+} flux (5.1 mmol m^{-2} d^{-1}) or 20–~54% of the directly measured flux (~13 mmol m^{-2} d^{-1}). The combined influence of reactions such as FeS, NH_4^+, and Mn^{2+} oxidation could therefore account for ~40–100% of the $CaCO_3$ dissolution (calcite and aragonite) during winter in LIS sediments.

Green and Aller (1998) report a mean diffusive O_2 flux into sediments during cruises

2–9 equivalent to 4.8 ± 2.3 mmol $m^{-2} d^{-1}$ (2.5–7.1 mmol $m^{-2} d^{-1}$). According to equation 10, the oxidation of 0.05 μmol FeS $cm^{-2} d^{-1}$ by O_2 between cruises 1–5 would account for an O_2 flux equivalent to 1.1 mmol $m^{-2} d^{-1}$. Likewise, oxidation of NH_4^+ and Mn^{2+} should result in O_2 uptake of ~0.6 and ~1.0 mmol $m^{-2} d^{-1}$ respectively (Eq. 10–11). Re-oxidation of FeS, NH_4^+, and Mn^{2+} is therefore equivalent to ~2.6 mmol O_2 $m^{-2} d^{-1}$ and represents ~37–100% of the wintertime O_2 flux. Oxidation of FeS, NH_4^+, and Mn^{2+} presumably accounts for <100% of sedimentary O_2 consumption as aerobic metabolism and additional reduced metabolite oxidation not accounted for here (Fe^{2+}, FeS_2) should also be responsible for a portion of the observed O_2 flux. The major conclusions are therefore that significant proportions of both total O_2 consumption and $CaCO_3$ dissolution during wintertime are accounted for by strong acid production and neutralization associated with re-oxidation reactions.

6. Conclusions

A regular seasonal pattern of diagenetic dissolution and biogenic precipitation of $CaCO_3$ occurs in central Long Island Sound muds. Multiple measurement techniques demonstrate that net dissolution of $CaCO_3$ dominates during winter, resulting in fluxes of dissolved Ca^{2+}, Sr^{2+}, and F^- out of the seafloor. Ca^{2+} release fluxes reach −20 mmol $m^{-2} d^{-1}$, averaging between ~ −5 (all method average) to −13 (directly measured) mmol $m^{-2} d^{-1}$ during winter. The highest fluxes occur when surface sediments are most undersaturated with respect to common carbonate minerals. A dramatic reversal of flux and net uptake of Ca^{2+} to the seafloor occurs in spring during recruitment of shell-bearing benthos, although dissolution continues to occur. Seasonal loss patterns of foraminifera tests from surface sediments require dissolution of at least ~7.4 mmol $m^{-2} d^{-1}$ $CaCO_3$ during wintertime. Stochiometric analyses of Ca^{2+}, Sr^{2+}, and F^- fluxes indicate that aragonite is a major carbonate dissolution source in addition lo-Mg calcite from foraminifera. Aragonitic mollusk shells are pitted and clearly dissolving. An additional source of F^- other than $CaCO_3$ dissolution, perhaps from Fe-oxide reduction, is likely. The dependence of net Ca^{2+} fluxes on sedimentary carbonate saturation states suggests dissolution reaction orders of n ~ 1–3 and whole sediment reaction rate constants of ~28–87 mmol $m^{-2} d^{-1}$ (~0.5–1.6% d^{-1}). Most biogenic carbonate (~90%) precipitated in LIS sediments each year is dissolved, equivalent to a loss of ~89 to 190 g $CaCO_3$ m^{-2} yr^{-1}. A significant proportion of dissolution, 40–100%, results from reoxidation of reduced metabolites and neutralization of strong acids. Large regions of muddy temperate estuaries presumably have carbonate cycling patterns comparable to central LIS.

Acknowledgments. We thank Josephine Aller, Magali Gerino, Ian Stupakoff, David Hirchsberg, and Kristen Sullivan for their assistance in the field. In addition, we thank the captain and crew of the R/V *Onrust* for getting us to where we needed to go. Margaret Lima, Rebecca Yingst and Steve Lucatuorto provided help in the laboratory. Josephine Aller, Cindy Lee, Bob Cerrato, Kirk Cochran, and Clare Reimers provided reviews of an early version of this manuscript. This research was

supported by Department of Energy grant DEFG0292ER61464 as part of the Ocean Margins Program and NSF grant OCE 9730933.

REFERENCES

Alexandersson, E. T. 1978. Destructive diagenesis of carbonate sediments in the eastern Skagerrak, North Sea. Geology, *6,* 324–327.

Aller, R. C. 1977. The influence of macrobenthos on chemical diagenesis of marine sediments. Ph.D. thesis, Yale University, New Haven, CT, 600 pp.

—— 1978. Experimental studies of changes produced by deposit feeders on pore water, sediment, and overlying water chemistry. Am. J. Sci., *278,* 1185–1234.

—— 1982. Carbonate dissolution in nearshore terrigenous muds: the role of physical and biological reworking. J. Geol., *90,* 79–95.

—— 1994. The sedimentary Mn cycle in Long Island Sound: Its role as intermediate oxidant and the influence of bioturbation, O_2, and C_{org} flux on diagenetic reaction balances. J. Mar. Res., *52,* 259–294.

Aller, R. C. and J. K. Cochran. 1976. $^{234}Th/^{238}U$ Disequilibrium in near-shore sediment: Particle reworking and diagenetic time scales. Earth Planet. Sci. Lett., *29,* 37–50.

Archer, D., S. Emerson and C. Reimers. 1989. Dissolution of calcite in deep-sea sediments: pH and O_2 microelectrode results. Geochim. Cosmochim. Acta, *53,* 2831–2846.

Baker, P. A., J. M. Gieskes and H. Elderfield. 1982. Diagenesis of carbonates in deep-sea sediments: evidence from Sr/Ca ratios and interstitial dissolved Sr^{2+} data. J. Sed. Petrol., *52,* 0071–0082.

Benninger, L. K., R. C. Aller, J. K. Cochran and K. K. Turekian. 1979. Effects of biological sediment mixing on the ^{210}Pb chronology and trace metal distribution in a Long Island Sound sediment core. Earth Planet. Sci. Lett., *43,* 241–259.

Berelson, W. M., D. E. Hammond and G. A. Cutter. 1990. *In situ* measurements of calcium carbonate dissolution rates in deep-sea sediments. Geochim. Cosmochim. Acta, *54,* 3013–3020.

Berelson, W. M., D. E. Hammond, J. McManus and T. E. Kilgore. 1994. Dissolution kinetics of calcium carbonate in equatorial Pacific sediments. Global Biogeochem. Cycles, *8,* 219–235.

Berner, R. A. 1980. Early diagenesis—A Theoretical Approach, Princeton Univ. Press, Princeton, NJ, 241 pp.

Bokuniewicz, H. J. and R. B. Gordon. 1980. Sediment transport and deposition in Long Island Sound. Adv. Geophy., *22,* 69–104.

Buzas, M. A. 1965. The distribution and abundance of foraminifera in Long Island Sound. Smithson. Misc. Collect., *149,* 1–89.

Carpenter, R. 1969. Factors controlling the marine geochemistry of fluorine. Geochim. Cosmochim. Acta, *33,* 1153–1167.

Emerson, S. and M. Bender. 1981. Carbon fluxes at the sediment-water interface of the deep-sea: calcium carbonate preservation. J. Mar. Res., *39,* 139–162.

Gerino, M., R. C. Aller, C. Lee, J. K. Cochran, J. Y. Aller, M. A. Green and D. Hirschberg. 1998. Comparison of different tracers and methods (*in situ,* laboratory) used to quantify bioturbation during a spring bloom: ^{234}Thorium, luminophores and Chl-*a.* Estuar. Coast Shelf Sci., *46,* 531–547.

Gieskes, J. M. 1974. The alkalinity-total carbon dioxide system in seawater, *in* The Sea, 5, E. D. Goldberg, ed., J. Wiley & Sons, 123–151.

Glover, C. P. and S. M. Kidwell. 1993. Influence of organic matrix on the post-mortem destruction of molluscan shells. J. Geol., *101,* 729–747.

Goldhaber, M. B., R. C. Aller, J. K. Cochran, J. K. Rosenfeld, C. S. Martens and R. A. Berner. 1977. Sulphate reduction, diffusion and bioturbation in Long Island Sound sediments: Report of the FOAM group. Am. J. Sci., *277,* 193–237.

Green, M. A. 1996. The biogeochemical mechanisms driving calcite and aragonite saturation states in Long Island Sound sediments: the effects on juvenile bivalves, foraminifera, and carbonate debris preservation. Ph.D. thesis, State University of New York, Stony Brook, NY, 257 pp.

Green, M. A. and R. C. Aller. 1998. Seasonal patterns of carbonate diagenesis in nearshore terrigenous muds: relation to spring phytoplankton bloom and temperature. J. Mar. Res., *56,* 1097–1123.

Green, M. A., R. C. Aller and J. Y. Aller. 1992. Experimental evaluation of the influences of biogenic reworking on carbonate preservation in nearshore sediments. Mar. Geol., *107,* 175–181.

——— 1993. Carbonate dissolution and temporal abundances of foraminifera in Long Island Sound sediments. Limnol. Oceanogr., *38,* 331–345.

——— 1998. The influence of carbonate dissolution on the survival of shell-bearing meiobenthos in nearshore sediments. Limnol. Oceanogr., *43,* 18–28.

Hales, B. 1995. Calcite dissolution on the seafloor: An *in situ* study. Ph.D. Thesis, University of Washington, Seattle, WA, 165 pp.

Hales, B. and S. Emerson. 1997. Evidence in support of first-order dissolution kinetics of calcite in seawater. Earth Planet. Sci. Lett., *148,* 317–327.

Hales, B., S. Emerson and D. Archer. 1994. Respiration and dissolution in the sediments of the western North Atlantic: estimates from models of *in situ* microelectrode measurements of pore water oxygen and pH. Deep-Sea Res., *41,* 695–719.

Jahnke, R. A., D. B. Craven and Jean-Francois Gaillard. 1994. The influence of organic matter diagenesis on $CaCO_3$ dissolution at the deep-sea floor. Geochim. Cosmochim. Acta, *58,* 2799–2809.

Jahnke, R. A., D. B. Craven, D. C. McCorkle and C. E. Reimers. 1997. $CaCO_3$ dissolution in California continental margin sediments—The influence of organic matter remineralization. Geochim. Cosmochim. Acta, *61,* 3587–3604.

Keir, R. S. 1980. The dissolution kinetics of biogenic calcium carbonates in seawater. Geochim. Cosmochim. Acta, *44,* 241–252.

Li, Y. H. and S. Gregory. 1974. Diffusion of ions in sea water and in deep-sea sediments. Geochim. Cosmochim. Acta, *38,* 703–714.

Mackin, J. E., R. C. Aller and W. J. Ullman. 1988. The effects of iron reduction and non steady-state diagenesis on iodine, ammonium, and boron distributions in sediments from the Amazon continental shelf. Cont. Shelf Res., *8,* 363–386.

Mackin, J. E. and K. T. Swider. 1989. Organic matter decomposition pathways and oxygen consumption in coastal marine sediments. J. Mar. Res., *47,* 681–716.

Martin, W. R. and G. T. Banta. 1992. The measurement of sediment irrigation rates: A comparison of the Br^- tracer and $^{222}Rn/^{226}Ra$ disequilibrium techniques. J. Mar. Res., *50,* 125–154.

Martin, W. R., A. P. McNichol and D. C. McCorkle. 2000. The radiocarbon age of calcite dissolving at the sea floor: Estimates from pore water data. Geochim. Cosmochim. Acta, *64,* 1391–1404.

McNichol, A. P., C. Lee and E. R. M. Druffel. 1988. Carbon cycling in coastal sediments: 1. A quantitative estimate of the remineralization of organic carbon in the sediments of Buzzards Bay, MA. Geochim. Cosmochim. Acta, *52,* 1531–1543.

Milliman, J. D. 1974. Recent Sedimentary Carbonates 1, Marine Carbonates. Springer-Verlag, Berlin, Germany, 375 pp.

Morse, J. W. 1983. The kinectics of calcium carbonate dissolution and precipitation. Rev. Mineral., *11,* 227–264.

Morse, J. W. and F. T. Mackenzie. 1990. Geochemistry of Sedimentary Carbonates, Elsevier Science Publishers, NY, 707 pp.

Morse, J. W., J. J. Zullig, L. D. Bernstein, F. J. Millero, P. Milne, A. Mucci and Gregory R. Choppin.

1985. Chemistry of calcium carbonate-rich shallow water sediments in the Bahamas. Am. J. Sci., *285,* 147–185.

Murray, J. W. and E. Alve. 1999. Natural dissolution of modern shallow water benthic foraminifera: taphonomic effects on the palaeoecological record. Palaeogeogr. Palaecol. *146,* 195–209.

Reaves, C. M. 1986. Organic matter metabolizability and calcium carbonate dissolution in nearshore marine muds. J. Sed. Petrol., *56,* 486–494.

Rude, P. D. and R. C. Aller. 1991. Fluorine mobility during early diagenesis of carbonate sediment: An indicator of mineral transformations. Geochim. Cosmochim. Acta, *55,* 2491–2509.

——— 1993. The influence of Mg^{2+} on the adsorption of fluoride by hydrous oxides in seawater. Am. J. Sci., *293,* 1–24.

Ruttenberg, K. C. 1990. Diagenesis and burial of phosphorus in marine sediments: Implications for the marine phosphorus budget, Ph.D. dissertation, Yale University, New Haven, CT, 375 pp.

Sanders, H. L. 1956. Oceanography of Long Island Sound, 1952–1954. X. The biology of marine bottom communities. Bull. Bingham Oceanogr. Coll., *15,* 345–414.

Tsunogai, S., M. Nishimura and S. Nakaya. 1968. Complexometric titration of calcium in the presence of larger amounts of magnesium. Talanta, *15,* 385–390.

Vanderborght, J. P., R. Wollast and G. Billen. 1977. Kinetic models of diagenesis in disturbed sediments. Part I. Mass transfer properties and silica diagenesis. Limnol. Oceanogr., *22,* 787–793.

Walter, L. M. and E. A. Burton. 1990. Dissolution of recent platform carbonate sediments in marine pore fluids. Am. J. Sci., *290,* 601–643.

Walter, L. M. and J. W. Morse. 1985. The dissolution kinetics of shallow marine carbonates in seawater: A laboratory study. Geochim. Cosmochim. Acta, *49,* 1503–1513.

Walton, W. R. 1952. Techniques for the recognition of living foraminifera. Contrib. Cushman Found. Foram. Res., *3,* 55–60.

Received: *15 November, 2000;* revised: *2 July, 2001.*